Production of iron-peptide complexes from spent yeast for nutraceutical industry

Check for updates

Ana Sofia Oliveira[a], Carlos M.H. Ferreira[a,b,∗], Joana Odila Pereira[a,b],
Sérgio Sousa[a], Margarida Faustino[a], Joana Durão[a,b],
Ana Margarida Pereira[a,b], Manuela E. Pintado[a], Ana P. Carvalho[a]

[a] Universidade Católica Portuguesa, Centro de Biotecnologia e Química Fina, Laboratório Associado, Escola Superior de Biotecnologia, Rua Diogo Botelho 1327, Porto 4169-005, Portugal
[b] Amyris Bio Products Portugal Unipessoal Lda, Portugal

ARTICLE INFO

ABSTRACT

Iron (Fe) deficiencies are a major health condition concern and over the years many solutions in the form of Fe supplementation have been investigated. Organic Fe-complexes are the most promising for Fe deficiencies remediation. The aim of present study was to value peptide rich waste streams from β-glucan and mannan production from spent yeast (Gpep and Mpep, respectively) as Fe-peptide complexes for Fe supplementation. These waste streams were first subjected to ultrafiltration treatment before assessing the capacity of these fractions to complex Fe was evaluated, without, and with nitrogen. Results have shown that Gpep > 1 kDa was the best fraction with a optimal pH of 6.0 and a time of 30 min. The resulting Fe-peptide complex was characterized using powder XDR, fluorescence, FTIR, SEM and Mastersizer Laser Diffraction. Results have shown that Gpep and Mpep waste streams have potential application as Fe supplementation in the form of Fe peptide complexes.

1. Introduction

Iron (Fe) is an important micronutrient in human nutrition, as it is involved in many biochemical processes in human metabolism such as oxygen transport, electron transfer reactions, gene regulation, and cell growth and differentiation (Waldvogel-Abramowski et al., 2014).

Given its importance in human metabolism, health problems may arise if not enough Fe is ingested. In fact, Fe deficiency is a major concern and one of the most widespread micronutrient deficiencies globally (Zhang et al., 2021). According to the World Health Organization (WHO) about 1.62 billion people suffered from anaemia, a form of Fe deficiency in blood cells, with greater prevalence in developing countries (World Health Organization, 2008). More recent numbers report that 30% of women aged between 15 and 49 years and 40% of children under 5 years suffered from anaemia in 2019 (WHO, 2021), while other estimates place the global age-standardized point prevalence of anaemia at around 23% (Safiri et al., 2021).

Although adults lose low amounts of Fe daily, 1–2 mg for man and woman, respectively (Collins and Anderson, 2012; Eckert et al., 2016), adequate quantities of Fe must be ingested in order to maintain Fe homeostasis. This is especially

important considering that only 5–18% of Fe naturally present in food is absorbed by the human body during the gastrointestinal digestion (Eckert et al., 2016). Factors such as living standards, food choices and food quality may also impact the levels of Fe absorbed by an individual; for example, plant-based Fe sources are less bioavailable than animal-based ones (Athira et al., 2021).

Fe supplementation in the diet is an effective way to address the problem of its deficiency, particular in cases where Fe bioavailability in diet is low. Elemental Fe and certain common Fe salts, such as Fe sulphate, carbonate, citrate, and fumarate, are commonly used in food fortification (Fairweather-Tait and Teucher, 2002). However, these salts have some drawbacks. First, these forms of Fe have low bioavailability (Athira et al., 2021; Zhang et al., 2021), and the consequently high amounts of Fe required to rectify Fe deficiency can cause health issues such as production of reactive oxygen species (ROS) species (Caetano-Silva et al., 2015), Fenton reactions, gastrointestinal irritation, vomiting, lethargy, grey cyanosis, pneumonitis, convulsions, coma and even death in extreme cases (Jeppsen and Borzelleca, 1999). Secondly, these simple salt forms can interact with food components, causing perceived changes in food properties such as flavour, colour or texture (Shubham et al., 2020).

One potential solution to these problems is the use of Fe-peptide complexes. These complexes are described as being more bioaccessible, bioavailable and safe than the aforementioned Fe salts (Wu et al., 2020). Their increased bioaccessibility is due to the competition of peptides with other organic molecules, such as phytates, tannins, oxalates and polyphenols, which can precipitate Fe at physiological pH (Anderson et al., 2018; Eckert et al., 2016; Lazarte et al., 2015; Lee and Song, 2009; Wu et al., 2020). Some reported results also show that organic forms of Fe have greater absorption rates than inorganic forms, although they are still limited by their carrier capacity (Zhang et al., 2017). Finally, safety is also cited as a reason for the preference of Fe-peptide complexes over other forms of Fe supplementation (Caetano-Silva et al., 2020; Wu et al., 2020).

Several sources of peptides have been tested recently, including whey protein (Athira et al., 2021; Caetano-Silva et al., 2017, 2015; O'Loughlin et al., 2015), mung beans (Budseekoad et al., 2018; Zhang et al., 2021), Antarctic krill (Wang et al., 2020), maitake (*Grifola frondosa*) (Yuan et al., 2019), casein digest (Smialowska et al., 2017), Pacific cod skin (Wu et al., 2017), sea cucumber (*Stichopus japonicus*) ovum hydrolysates (Sun et al., 2017), Alaska pollock skin (*Gadus chalcogrammus*) (Chen et al., 2017; Guo et al., 2015, 2013), sugar cane (de la Hoz et al., 2014b), anchovy (Wu et al., 2012), and chickpea (Torres-Fuentes et al., 2012), among others. A common reason for choosing a particular peptide source is to valorize protein-rich sub- and by-products from other processes, thus promoting circular economy. One protein-rich byproduct that has received attention is brewer's yeast, *Saccharomyces cerevisiae* (Oliveira et al., 2022a). With the increasing use of yeast in beverage industry (Bombe, 2019) and synthetic biology, among others, large quantities of yeast waste are generated yearly. As of 2020, world beer production was estimated at nearly 2 billion hectolitres (Conway, 2021), generating ca. 4–8 million tonnes of yeast waste (Oliveira et al., 2022b).

To valorize spent yeast, various processes have been developed to produce new and valued products. These processes include the production of mannans and β-glucans from yeast waste (Faustino et al., 2021; Freimund et al., 2003; Liu et al., 2008; Tian et al., 2019). However, besides creating valued products, these processes also generate protein-rich waste that needs further processing or treatment.

Motivated by the desire to create new, healthy, effective, and safe Fe-peptide complexes for the nutraceutical industry of Fe supplementation, and by the need to further process and add value to these by-products, the viability of using these protein-rich wastes as sources for Fe-peptide complexes was studied. To this end, these by-products were first sorted by size into different molecular weight (MW) peptide fractions, increasing their protein purity. These fractions were then tested for their viability as mineral chelating agents. Variables such as pH, time, protein-to-Fe ratio and oxidative conditions were also studied and evaluated. Finally, the physicochemical characterization of Fe-peptide complexes was performed to understand the complexation behaviour and final product properties.

2. Material and methods

2.1. Peptide fractions production by ultrafiltration

Peptide fractions were produced from protein-rich wastes of β-glucan (Gpep) and mannan (Mpep) extractions (Freimund et al., 2003; Liu et al., 2008; Tian et al., 2019) from engineered spent yeast (*S. cerevisiae*) used in Amyris facilities to produce farnesene (Emeryville, California, USA). The supernatants of yeast β-glucan and mannan extractions were subjected to ultrafiltration using an Ultracel® 1 kDa ultrafiltration disc (regenerated cellulose, 76 mm diameter) (Merck KGaA, Darmstadt, Germany) in an Amicon® stirred cell model (Merck KGaA, Darmstadt, Germany) to separate peptides by size, resulting in different MW peptide fractions. After the first step of 1 kDa ultrafiltration, the retentate was diafiltrated with 3 volumes of deionized water to increase the protein purity of final fractions (Supplementary material 1 – S1). At the end of ultrafiltration process, samples were freeze-dried (Freeze-dryer Alpha 2–4 LSCbasic, Martin Christ, Osterode am Harz, Germany). As demonstrated in S1, this process allowed to obtain a total of 3 different MW peptide fractions for each waste stream: retentate "Gpep > 1 kDa" and permeates "Gpep < 1 kDa FS" (first ultrafiltration permeate fraction) and "Gpep < 1 kDa DF" (diafiltration permeate fraction) from β-glucan, and retentate "Mpep > 1 kDa" and permeates "Mpep < 1 kDa FS" and "Mpep < 1 kDa DF" from mannans.

2.2. Chemical characterization of peptide fractions

2.2.1. Protein and dry weight quantification

Pierce™ BCA protein assay kit (Thermo Fisher Scientific Inc., Massachusetts, USA) was used for protein determination of fractions in 96 well microplates. This method is based on the production of a purple-coloured product by the reduction of Cu^{2+} to Cu^{1+} by proteins in alkaline medium, followed by Cu^{1+} reaction with bicinchoninic acid (BCA). This reaction product can be read at 562 nm after 30 min in a microplate reader (Synergy H1, Biotek Instruments, Winooski, USA).

According to the Association of Official Analytical Chemists standard protocols, dry weight was determined at 105 ºC for 24 h (AOAC, 2005).

2.3. Fe-peptides complexation

2.3.1. Fraction initial screening - reaction without nitrogen

An initial complexation screening was performed using the protocol of Caetano-Silva et al. (2015) with some modifications. Each peptide-rich fraction was prepared at 0.2% protein (w/w) in deionized water and 0.1% of Fe (w/w) (FeSO$_4$.7H$_2$O; Sigma-Aldrich, Inc., St. Louis, USA) was added to the solution under stirring, corresponding to protein:Fe ratio of 2:1. The solution was stirred for one hour with the pH monitored and adjusted periodically to 7.0. In the end, the solution was centrifuged (12000g, 5 min) and the supernatant was filtered (ø = 0.45 µm; Chromafil® PET-45/25, Macherey-Nagel, Germany). The soluble Fe from the resulting solution was measured by ICP-OES. Each extract was tested in triplicate and the results expressed as a percentage of the total added Fe (% of initial), are presented as an average of n = 3.

2.3.2. Complex formation – anoxic conditions

2.3.2.1. Experimental setup. A schematic of the experimental setup used for the complexation reaction in the presence of a nitrogen atmosphere is displayed in Fig. 1A.

A three necked 500 mL flask was used for the purpose. When not in use, the flask necks would be closed using the appropriate stoppers. The middle neck was used to insert a pH electrode for live control, and one of the side necks was used to insert the NaOH probe of Automatic Potentiometric Titrator AT-710 system (Kyoto Electronics Manufacturing Co. Ltd, Japan) to adjust pH during reaction. The second side neck was used to insert a nitrogen line. The flask was placed in a magnetic stirrer and a magnetic bar was inserted in the flask to stir the solution during the reaction.

2.3.2.2. Reaction protocol. A peptide-rich solution was prepared to a protein concentration of 0.02% (w/w) and placed in the reaction flask. Nitrogen gas was purged for 10 min and 0.01% of Fe (w/w) was added while the solution was continuously stirred and purged for more 10 min. Finally,

the pH of the solution was slowly increased to pH 7.0. For the next 30 min, the solution was kept under nitrogen purge and the pH was monitored and adjusted to 7.0 accordingly. At the end of reaction, the solution was collected in a flask under a nitrogen atmosphere and stored at room temperature overnight. In the next day, the pH of solution was adjusted back to pH 7.0, followed by centrifugation (12000g, 5 min) and filtration for some precipitate remotion (ø = 0.45 µm). The soluble Fe from the resulting solution was measured by ICP-OES. Each reaction was performed in triplicate and the results expressed as a percentage of the total added Fe (% of initial), are presented as an average of n = 3. Blank experiments were also carried out, where the same conditions were tested, in duplicate, in the absence of peptide extracts.
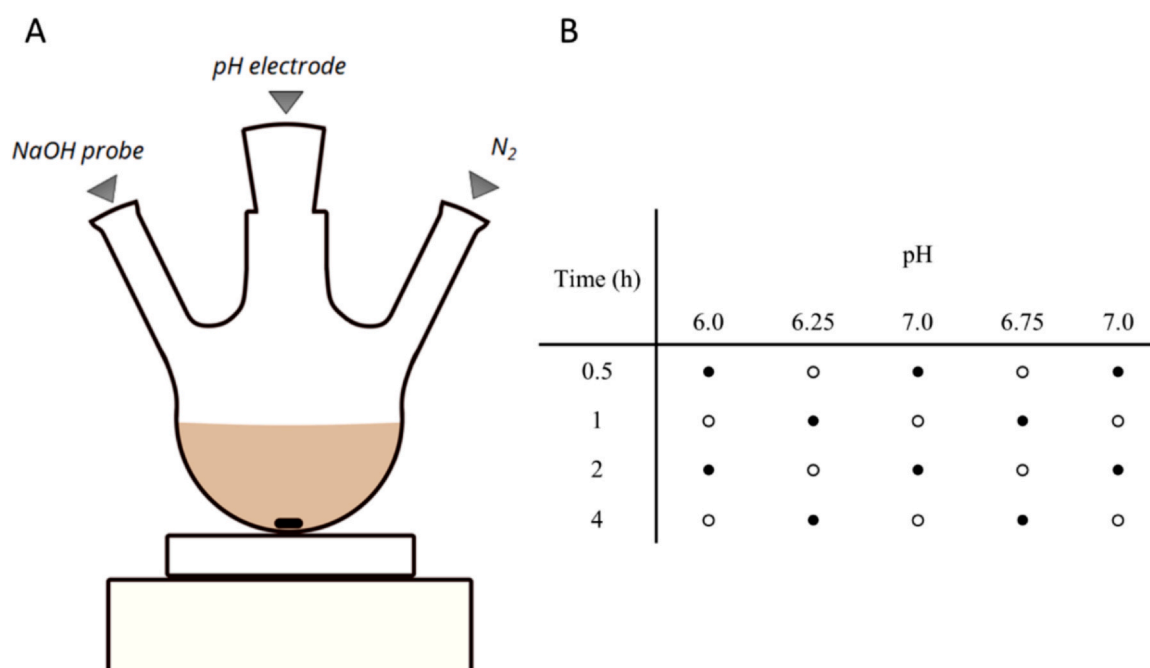
2.3.2.3. Factorial design and statistical analysis. To find the optimal complexation conditions, a two-factor factorial design was used. The effect of pH was studied at five different levels (6.00, 6.25, 6.50, 6.75 and 7.00) while time was varied at four levels (0.5, 1.0, 2.0 and 4 h). As to reduce the number of conditions, only 50% of the total possible combinations were performed, as shown in Fig. 1B. Each combination was performed in triplicate. Experiments were conducted in a randomized order.

To model the response of % of complexed Fe to the tested factors, the following second-order polynomial model was chosen:

$$Y = b_0 + b_1 X_1 + b_2 X_2 + b_3 X_1 X_2 + b_4 X_1^2 + b_5 X_2^2 + \epsilon$$

Where Y is the percentage of the initial Fe in solution after complexation reaction, b_i represent the different coefficients of each factor, X_i represent pH and time factors and ϵ the random experimental error.

The model was fitted using the Real Statistics Resource Pack software (Release 7.2) with multivariate regression as the optimization and fitting method. To analyze extreme data points of the regression fit and determine their validity, the Cook's D method was applied. Data points with a value

Fig. 1 – A: Experimental design of the complexation reaction setup using nitrogen (N$_2$), pH control and NaOH probe. **B:** Conditions of pH and time on the complexation reaction efficiency assays. •: combination tested; ○: combination not tested.

greater than 0.2 were considered for removal from the regression, and the regression was conducted a second time.

2.3.3. Fe determination by ICP-OES

Fe content was measured according to the procedure of Chatelain et al. (2014) with some modifications in an optical emission spectrometer Model Optima 7000 DV ™ ICP-OES (Dual View, PerkinElmer Life and Analytical Sciences, Shelton, CT, USA) with radial configuration. The analysis was done in triplicate and Fe was calculated according to Fe standard calibration curve from 0.05 to 10 mg/L of commercial mix standard for ICP analysis (Inorganic Ventures, Christiansburg, USA). Before ICP analysis, a microwave digestion of samples (2 mL) was conducted in a speedwave XPERT (Berghof Products + Instruments GmbH, Eningen, Germany) using 5 mL of Suprapur® HNO_3 and 2 mL of 35% H_2O_2 (Merck KGaA, Darmstadt, Germany). The digestion protocol consisted of five steps: 1) 160 °C/5 min, 2) 190 °C/ 10 min, 3) 190 °C/10 min, 4) 100 °C/2 min and 5) 100 °C/2 min. The digested samples were then diluted to 25 mL with ultrapure water for ICP-OES analysis.

2.4. Complex characterization

2.4.1. X-ray diffraction (XRD)

The diffraction of X-rays was analysed using an X-ray diffractometer (Rigaku MiniFlex 600, Tokyo, Japan). Freeze dried samples were packed in a sample plate and measured using the following conditions: Cu kα radiation, operated at 40 kV and 15 mA, with 2θ range from 3° to 80°, a scanning speed of 3° min^{-1}, and a step of 0.01°.

2.4.2. Intrinsic fluorescence

The intrinsic fluorescence emission spectra were recorded using a Synergy H1 microplate reader (Biotek Instruments, Winooski, USA). A wavelength of 280 nm was used for excitation of samples and emission wavelengths from 300 to 400 nm were recorded in of 5 nm increments. Samples were measured in triplicate and the results were expressed as an average.

2.4.3. Fourier-transform infrared (FTIR) spectroscopy

A diamond crystal of attenuated total reflectance (ATR) assembly Perkin-Elmer Frontier FTIR spectrometer coupled with a Universal ATR Sampling Accessory (Massachusetts, USA) was used to obtain infrared spectra. Samples were measured in a wave number range between 4000 and 550 cm^{-1} with a resolution of 1 cm^1.

2.4.4. Scanning Electron Microscopy (SEM)

The samples morphology was evaluated using a Phenom XL G2 (Thermo Fischer Scientific, The Netherlands) scanning electron microscope (SEM). Sample powders were placed over double-sided adhesive carbon tape (NEM tape; Nisshin, Japan), which covered the observation pins, and were coated with gold/palladium on a sputter coater (Polaron, Germany).

An acceleration voltage of 5 kV in high-vacuum mode was used and all images are representative of the morphology of each sample.

2.4.5. Particle size

The particle size distribution was assessed using a Malvern Mastersizer 3000 - Laser Diffraction (Malvern Instruments Ltd., UK) with a refractive index of 1.40 and absorption of 0.01 parameters selected. Ethanol absolute was used as dispersant. According to the laser diffraction through the particles of material, a scattering pattern was generated and then used to calculate the particle size via Mie theory.

3. Results and discussion

3.1. Protein content

The supernatants of yeast β-glucan and mannan extractions were submitted to 1 kDa ultrafiltration and diafiltrated and the protein concentration of the peptide-rich fractions was determined thereafter. A protein content ranging 23.0–86.4% (w/w) was found, as shown in Table 1. Additional nutritional characterization of peptide-rich fractions (Gpep/Mpep > 1 kDa and Gpep/Mpep DF < 1 kDa) can be found in our previous work (Oliveira et al., 2022c).

Several authors have used membrane filtration to produce peptide fractions with low MW, since these are described as better ligands for mineral binding (Caetano-Silva et al., 2018; de la Hoz et al., 2014a, 2014b; O'Loughlin et al., 2015; Yuan et al., 2019). The high selectively and efficiency together with low energy consumption makes it quite appealing to food industry (Marson et al., 2020). In fact, for ideal Fe complexation, peptides should be ranging in size from 300 to 1500 Da (Caetano-Silva et al., 2020). Our peptide-rich fractions appear to be promising candidates, since our previously study revealed approximately 80–90% of peptides under 1 kDa in Gpep and Mpep FS < 1 and 30–60% in Gpep and Mpep > 1 (Oliveira et al., 2022c). Worth noting that the large percentage of peptides under 1 kDa observed in both Gpep and Mpep > 1 kDa may be attributed to the limited selectively of ultrafiltration cut-off membranes, as explained in our previous article. As a result, the first step of this study was to evaluate the complexation capacity of different MW fractions produced. The peptide rich solutions for the following complex reactions were prepared according to the protein concentrations listed above (Table 1).

3.2. Fraction complexation capacity screening

The values of soluble Fe(II) found at the end of the one hour reaction, as measured by ICP-OES, are found in Fig. 2A. Almost all reactions resulted in less than 10% of the initial Fe remaining in solution, with exception of Gpep < 1 kDa DF and Mpep < 1 kDa DF, with 10.65% and 10.04% respectively. The lowest amount of Fe in solution was found at the

	Gpep			Mpep		
	> 1 kDa	FS < 1 kDa	DF < 1 kDa	> 1 kDa	FS < 1 kDa	DF < 1 kDa
Protein (%)	67.2 ± 16.0	23.0 ± 1.3	67.6 ± 25.6	86.4 ± 8.7	44.8 ± 5.8	48.3 ± 15.9

Table 1 – Protein concentration (% w/w) of peptide-rich fractions.

Results are expressed in average ± standard deviation (n = 4).
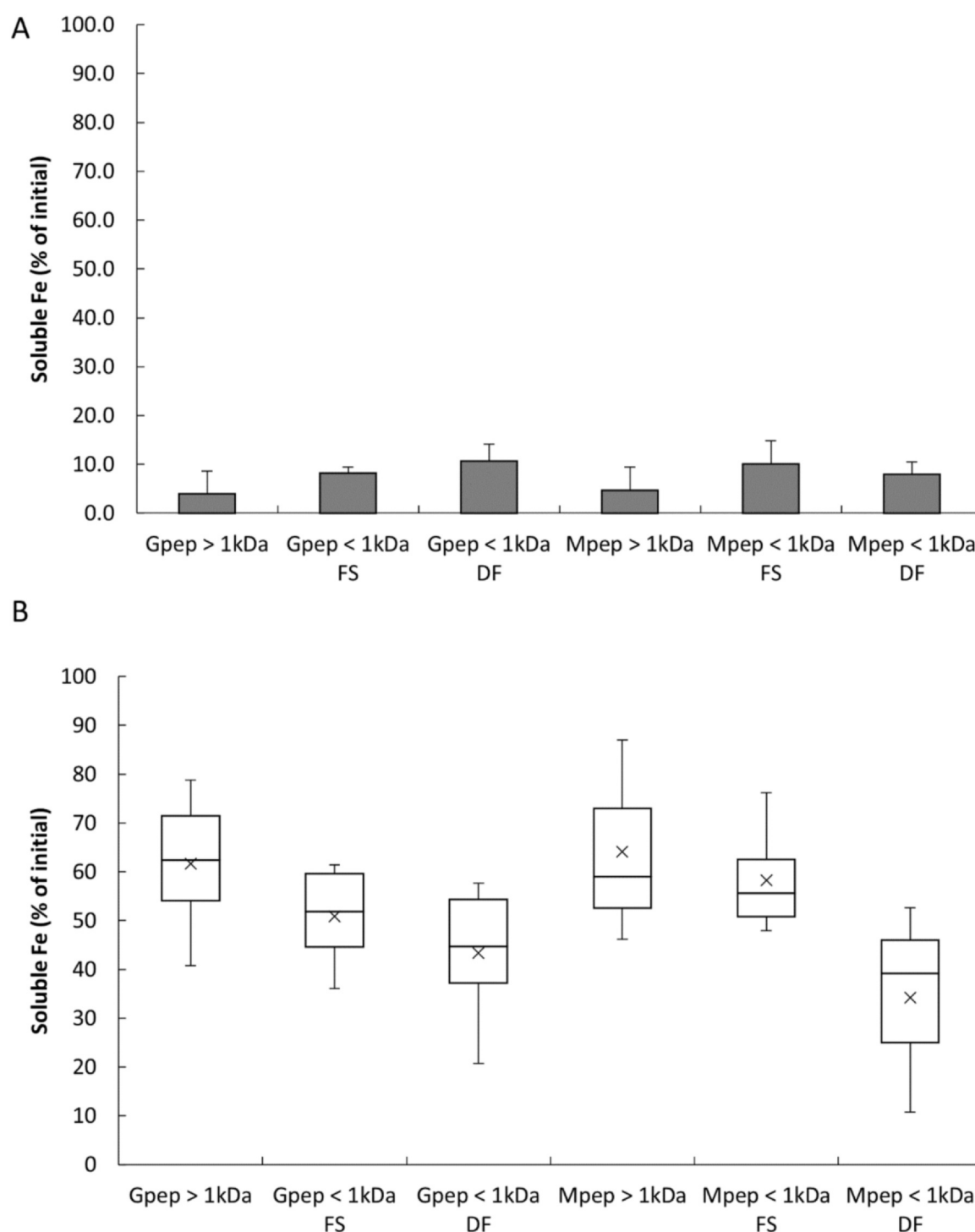
Fig. 2 – A: Average (n = 2) soluble Fe found in solution after complexation reaction with no nitrogen atmosphere expressed as percentage of the initial added Fe, bars represent standard deviation. B: Soluble Fe found in solution after complexation reaction with solution purge and nitrogen atmosphere expressed as percentage of the initial added Fe. Boxplots with minimum, Q1, median, Q3 and maximum. Crosses: average value (n = 6). Gpep: supernatant from β-glucans procedure; Mpep: Ethanol supernatant from mannans procedure; > 1 kDa: fraction retained in ultrafiltration; < 1 kDa FS: first ultrafiltration permeate fraction; < 1 kDa DF: diafiltration permeate fraction.

concentrated fractions (> 1 kDa) of both by-products, with 3.92% and 4.68% for Gpep and Mpep, respectively.

During the complexation reaction under normal conditions, the pH was very unstable for at least the first 30 min, consistently decreasing as it was adjusted to 7.0. At the same time, the formation of a precipitate was observed as NaOH was added to the solutions to adjust the pH to the required value.

There are two factors that may be responsible for the decrease in pH. One possibility is that ferrous Fe (II) may be at its solubility limit and precipitate out as $Fe(OH)_2$ (Monhemius, 1977), depleting hydroxide from solution and thereby reducing pH. The constant stirring of the solution in open air may also contribute to the oxidation of ferrous Fe (II) into ferric Fe (III), which is even more insoluble at neutral pH (Monhemius, 1977). On the other hand, it is possible that

protons may be released by peptides and/or proteins as a result of the complexation and consequent change in pKa of some acid/base moieties (Onufriev and Alexov, 2013). However, the formation of a thick brown precipitate seems to support the first hypothesis.

The amount of soluble Fe found at the end of the reaction (Fig. 2A) also supports the previously discussed assumptions. Overall, the amount of Fe present in the solution is low, ranging from about 4–10.5%. Despite this range, statistical analysis reveals no differences between different fractions. Comparing these results with literature, they are somewhat low since Sun et al. (2017) have found values ranging from 15% to 90% of the added Fe in their samples. However, proteins of this study were extracted from other matrix, such as sea cucumber ovum hydrolysates. On the other hand, our values are in the same range as those found by Wu et al. (2017) using peptides from Pacific cod skin gelatin for complexation. Other sort of optimization was performed by Caetano et al. (2017) which allowed soluble Fe yields between 40% and 90% when using different Fe:protein ratios and working with whey protein hydrolysates. Also in this study, the authors tested different ultrafiltration fractions (filtrate and retentate) as well the original hydrolysate and, contrary to our study, found differences in complexation behaviour between different fractions (Caetano-Silva et al., 2017). Similarly, O'Loughlin et al. (2015) studied the complexation capacity of two whey protein hydrolysates that were subjected to an ultrafiltration cascade. The two fractions studied (30 kDa retentate and 1 kDa permeate) have shown slightly different behaviours, with a decrease in Fe solubility when reaching pH 7. Nonetheless, more than 80% of Fe remained soluble (O'Loughlin et al., 2015).

During the reactions under normal conditions, Fe oxidation was observed and the yield was consequently low. Therefore, new conditions were tested, including the use of an anoxic environment. In these reactions nitrogen gas was used to purge the reaction solution and the environment of the reaction was sealed under a nitrogen atmosphere. Under these conditions a different behaviour was observed. Precipitation still occurred, but to a lesser degree and with a different colour than in the first case (greenish instead of ochre). Also, pH variation was observed but to a lesser degree, being the solution much more stable than in the previous experiment. Overall, an improvement was observed, with larger amounts of soluble Fe still found, with values averaging from 39% (Mpep < 1 kDa) to 64% (Mpep > 1 kDa). This is in stark contrast to the previous results obtained under normal atmosphere conditions (Fig. 2). Interestingly, the permeate fractions (FS and DF) had less soluble Fe compared to the concentrate fractions which had the largest. In fact, it is possible to observe a trend in the data suggesting that the lower the size of peptides in solution, the less Fe is maintained in solution. However, this trend and differences between steps of filtration within the same by-product are not statistically significant (p > 0.05) possibility attributable to the large % of peptides MW under 1 kDa found in all fractions (Oliveira et al., 2022c).

In comparison with literature previously discussed, this data set is more comparable to that of Sun et al. (2017). However, lower percentages of soluble Fe than O'Loughlin et al. (2015) or Caetano-Silva et al. (2017), (2015) were still obtained, which may be related with two main complexation factors: interference of time (reaction and precipitation kinetics) and pH (protonation and complexation equilibria), as

reviewed by Caetano-Silva et al. (2020). These two factors were explored in more detail in the next experimental set.

### 3.3. Complex formation conditions optimization

An analysis in the literature reveals that different conditions for conducting Fe-peptide complexation have been explored. For example, Zhou et al. (2012) used seven different pH levels in the 5.0–8.0 pH range while Smialowska et al. (2017) tested three different pH from 2.75 to 6.7. While some works use a single pH value, the authors differ on the pH chosen. For example, the following values have been used: pH 5.0 (Wu et al., 2020; Yuan et al., 2019), pH 6.0 (Wang et al., 2020) or pH 7.0 (Caetano-Silva et al., 2017, 2015; Sun et al., 2017). However, most works focus on a 5–8 range, though a pH higher than 7.0 may not be desirable since a formation of precipitate was observed at the first screening assay. On the other end, a lower pH may compromise complexation, as fewer moieties will be deprotonated and available for complexation. For this reason, a pH ranging from 6.0 to 7.0 was chosen for our optimization study. Also, from the experience obtained in the previous experiments, the solution pH continuously decreases over time, even past one hour. In fact, in a test experiment (data not shown) that was conducted over the period of four hours, pH was still not fully stable. The observation that 24 h later the pH has decreased raises the question of what the ideal time for the complexation reaction is, and if it is pH dependent. Therefore, different times were also tested, ranging from 0.5 h to 4 h. Gpep > 1 kDa was the peptide fraction chosen for this optimization since "> 1 kDa" samples presented a high soluble Fe in the screening study and Gpep > 1 kDa had higher median values of soluble Fe found in the screening study.

Average values ($n = 3$) of soluble Fe at the end of the reaction for each set of conditions tested can be found in Table 2. The highest average value, 88.0%, was found at pH 6.0 and 0.5 h of reaction, followed by other low pH and low time reaction conditions. In fact, if the average values are plotted just considering pH or time alone (Figs. S2A and S2B, respectively), a trend of decreasing soluble Fe as pH increases can be observed, where at pH 7.0 values are similar to those found in the previous experiment. Regarding time, there is no clear trend, but the highest values are found for 1 h. However, time does not seem to have a large impact on the final solubility of Fe as pH has.

The fitting of out model using a multivariate regression analysis to the obtained data returns the following equation:

Table 2 – Average ± standard deviation (n = 3) soluble Fe found for each condition tested in the experimental factorial design used.		
pH	Time (h)	Complexed Fe (% of initial)
6.0	0.5	88.0 ± 3.1
6.0	2.0	86.4 ± 1.5
6.25	1.0	83.5 ± 6.7
6.25	4.0	65.8 ± 8.6
6.5	0.5	55.1 ± 8.6
6.5	2.0	73.3 ± 9.5
6.75	1.0	71.2 ± 5.5
6.75	4.0	41.7 ± 13.4
7.0	0.5	53.4 ± 6.3
7.0	2.0	36.2 ± 11.4
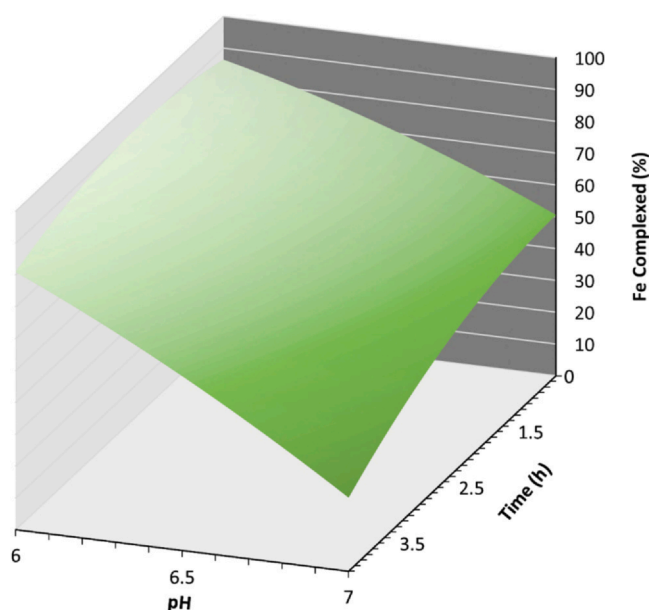
Fig. 3 – Response surface depicting soluble Fe (as % of initial added) versus time and pH. Model obtained from applying multivariate regression to complexation data, according to formula described in the main text.

$Fe_{complexed}$ (%)

$$= 32.27pH + 64.35t - 8.49pH \cdot t - 4.61pH^2 - 3.25t^2 + 50.04$$

With $R^2 = 0.794$ and $p < 0.0001$.

The corresponding response surface of the proposed model can be seen in Fig. 3 and the residuals of the multivariate regression in Fig. S3.

The results presented in Fig. 3 show the trend already observed in Figs. S1A and S1B. Within the tested intervals of pH and time, the model predicts pH as the most important factor affecting the outcome of the complexation reaction. Using a pH as high as 7.0 is not advantageous, as most Fe(II) will either precipitate or oxidate and readily precipitate, while pH 6 is more ideal, with the model predicting values around 80–90% complexed, in contrast to pH 7.0 with values around 20–55%.

Regarding time, its influence seems pH related. At lower pHs, the time influence is not very noticeable, as seen in Fig. 3, at pH 6.0, a 10% points difference from best to worst yields can be observed, with the greater difference at pH 7, where a 35% points difference is observed. The ideal time for complexation also changes slightly over pH, from 2 h at pH 6.0–1 h at pH 7.0. The observed changes may be linked to how precipitation kinetics and equilibria are affected by pH. At higher pH (7.0), the stability of Fe-peptide complexes decreases, leading to release of free Fe and peptides. The free Fe ions tend to precipitate more easily at this pH, due to more favourable conditions for precipitation to occur. Moreover, lower pH levels tend to increase the stability of the Fe-peptide complexes as noted by Ahile et al. (2020).

However, since the difference in yield between 0.5 h and 1 h reaction time at pH 6.0 was found to be minimal, the extra resources required for a longer reaction time (energy and nitrogen gas) were deemed unjustifiable for the small increase in yield observed. Consequently, a reaction time of 0.5 h and pH 6.0 were chosen as optimal conditions for complexation reactions of Fe(II) with Gpep > 1 kDa FD fraction.

3.4. Complex characterization

3.4.1. XRD

A powerful method for assessing the structural changes in peptides following complexation with metal ions is XRD analysis (Walters et al., 2018). As demonstrated by several studies, XRD can provide valuable information on conformational changes in peptides following complexation with metals such as Fe (Jin et al., 2011; Malison et al., 2021; Wang et al., 2018). Generally, peptide samples exhibit weak or no crystalline reflections, but instead a broad band at around 2θ 20°, which is characteristic of an amorphous sample. The presence of metal ions can result in changes on this spectrum, such as the appearance of sharp reflection bands, which are indicative of structural changes in the peptide (Walters et al., 2018).

The X-ray diffraction patterns of Gpep > 1 kDa, Gpep > 1 kDa-Fe and Fe hydroxides are depicted in Fig. 4. Fe precipitates from the reaction without Gpep > 1 kDa (blanks) were used as control for Fe (hydro)oxides. The Gpep > 1 kDa presents a major broad band centred around 2θ 20°, as expected. On the other hand, with the addition of Fe, Gpep > 1 kDa-Fe exhibits two strong crystal diffraction peaks, as well as some other small diffraction peaks. The two major peaks are found at 2θ 18.5° and 26°. The analysis of Fe precipitates spectrum reveals that these have a different pattern of crystallization than that of Gpep > 1 kDa-Fe, as evidenced by the increased number of reflections. There are four main peaks at 2θ 14.5°, 27.4°, 36.7° and 47.2°, which both differ in quantity as well as in angle of reflection. Similar results were found by Yang et al. (2019), where the Fe complexes created by the authors had a different XRD pattern compared to the original materials used, or by Zhu et al. (2018), although in the latter the signal difference was low due to the low crystallization level of the matrix.

3.4.2. Intrinsic fluorescence

The averaged spectra obtained for the three replicates of Gpep > 1 kDa-Fe complexes, as well as for Gpep > 1 kDa, can be seen in Fig. 5. It is possible to observe a decrease in the fluorescence band at 340 nm, caused by the addition of FeSO4 to Gpep > 1 kDa. This is likely due to the quenching of tryptophan residues in the peptide by Fe ions as noted by Wu et al. (2012). Furthermore, a red-shift in peak intensity from 340 nm to 345 nm is observed, this is also attributed to the quenching of tryptophan residues in the peptide by the Fe ions and is consistent with previous reports. For example Wu et al. (2012) have demonstrated that the addition of $FeSO_4$ to anchovy muscle protein resulted in a decrease in fluorescence between 310 nm and 400 nm, after excitation at 295 nm, while at the same time, registering a red-shift in the emission spectra. Similarly, β-lactoglobulin hydrolysates also showed a decrease in fluorescence intensity at the same wavelength when Fe salts were added, with a simultaneous red-shift in emission spectra (Zhou et al., 2012). On the other hand, Lin et al. (2021) did not register a red-shift in emission spectra, unlike other studies, while observing the reduction of intensity on fluorescence. These changes may be attributed to the conformational changes of peptides caused by complexation, which results in less exposure of tryptophan to solvent, resulting in an emission behaviour change (Walters et al., 2018).
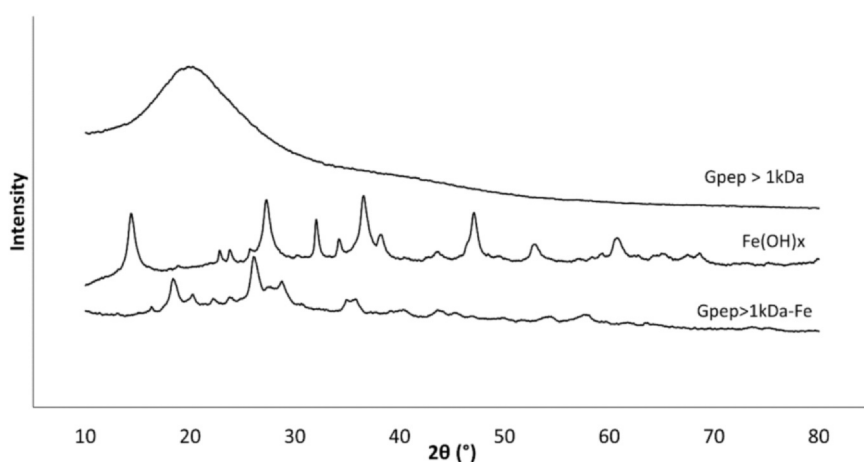
Fig. 4 – XRD patterns of Gpep > 1 kDa, Gpep > 1 kDa-Fe complex and Fe hydroxides (Fe(OH)x) from 3° to 80°.

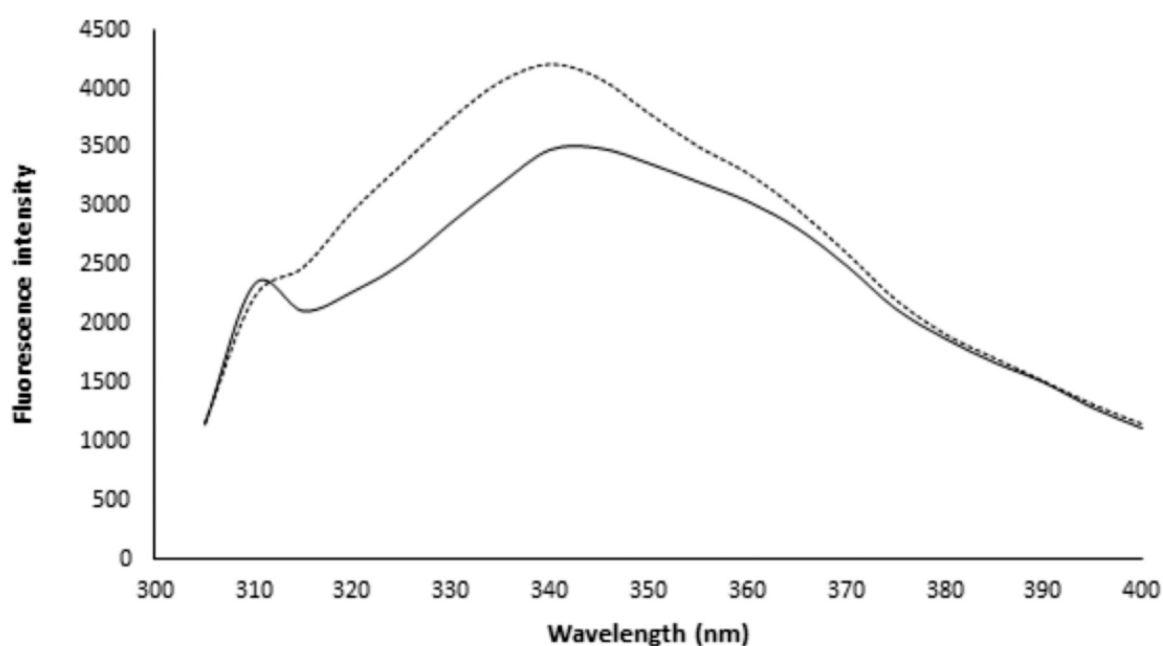**Fig. 5 – Average (n = 3) fluorescence emission spectra of Gpep > 1 kDa (dashed line) and Gpep > 1 kDa-Fe complexes (solid lines). Excitation wavelength = 280 nm; emission wavelength = 300–400 nm.**

3.4.3. FTIR spectroscopy

The study of new complexes with FTIR is common practice, given its easiness and simplicity of use. The information provided is also valuable since there are several functional groups that can take part in the complexation with Fe(II). Shifts in amides I, II and III, as well as in carboxyl (-COOH), hydroxyl (-OH), sulfhydryl (-SH), and methyl (-CH3) groups, usually part of peptide side chains, all may provide useful information regarding structural and chemical changes resulting from complexation (Walters et al., 2018). These changes, such as the appearance of new bands at specific wavenumbers, demonstrate the formation of covalent bonds between the peptide and the metal ions and a strong binding of the two entities. Therefore, the analysis of the comparison of FTIR spectra from un-complexed fraction and complexed fraction may be of help to evaluate how the peptides have complexed Fe(II).

The ATR-FTIR spectra for Gpep > 1 kDa, Gpep > 1 kDa-Fe complex and Fe hydroxides are presented in Fig. 6. The first major difference is the presence of two very intense and sharp bands in the Gpep > 1 kDa-Fe complex spectrum at

1075 and 599 cm^{-1}, whereas they are considerably smaller in the Gpep > 1 kDa spectrum. These bands are likely due to the presence of sulphate ions, as result of the added Fe sulphate salt for the complex formation (Coates, 2006). The influence of different counter ions in IR spectra has been previously described (Caetano-Silva et al., 2017), and the presence of this strong band makes it difficult to analyze the spectra in this region. Bands in the region of 500 cm^{-1} and 1100 cm^{-1} have been associated with the stretching vibration of N-Fe and C-O-Fe bounds, respectively (Caetano-Silva et al., 2017; Huang et al., 2011; Wu et al., 2017; Zhou et al., 2012). For example, Caetano-Silva et al. (2017) related a shift in the ν_sC-O bands from 1110 to 1039–1117 cm^{-1} to the formation of Fe-O-C bonds, while bands at 1430 and 1620 cm^{-1} were related to symmetric and asymmetric (respectively) stretching vibration of Fe-COO bonds (Caetano-Silva et al., 2017). On the other hand, Zhou et al. (2012) described the appearance of strong bands at wavelengths of 1086, 1181, and 1253 cm^{-1} which the authors attribute to the coordination of the C-O-Fe bond in the peptide-Fe complex, while relating the shift at 3408–3375 cm^{-1} to complexation at amine groups in the
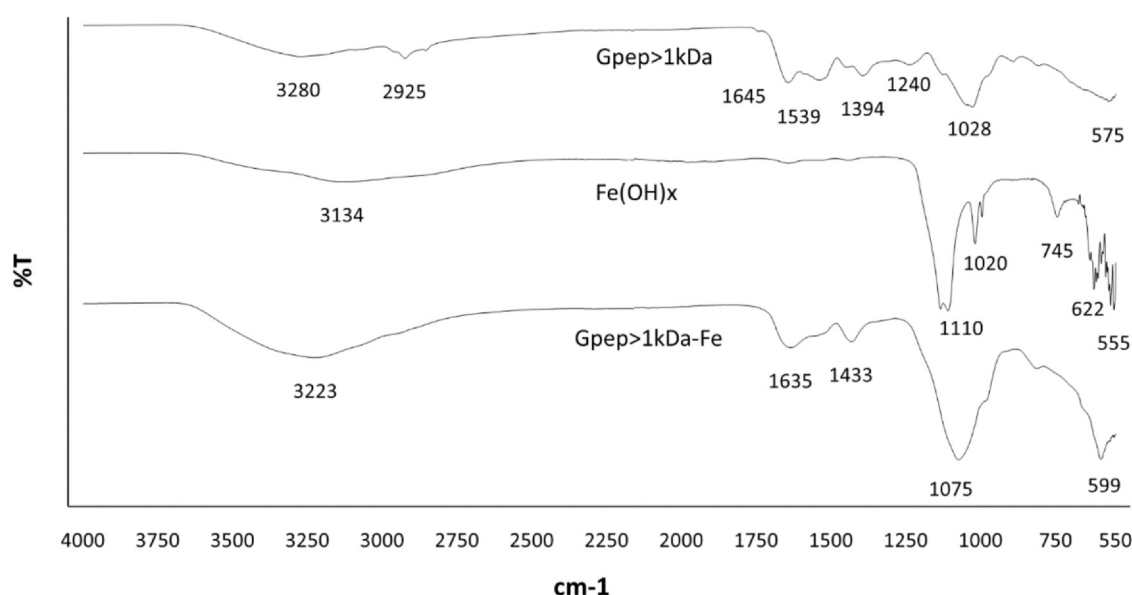
Fig. 6 – FTIR spectra of Gpep > 1 kDa, Gpep > 1 kDa-Fe complex and Fe hydroxides (Fe(OHx)) in the region from 4000 to 550 cm⁻¹ and identification of the main peaks observed.

peptide (Zhou et al., 2012). Observations in this range would be of practical importance, as they allow us to better understand the chemical interactions between the peptide and Fe ions but are obscured by the presence of the bands associated with sulphate ions.

Nonetheless, a number of band shifts were observed, providing insight into the specific interactions between the peptide and Fe ions. One of the most significant shifts observed was the shift of the band at 1433, from the original 1394 cm⁻¹ which can be attributed to carboxyl groups. This shift has been previously associated with a COO-Fe (Caetano-Silva et al., 2017). Additionally, changes were also observed in the Amide I and Amide II bands of Gpep > 1 kDa, found at 1645 and 1539 cm⁻¹ respectively. The Amide I band shifted from 1645 to 1635 cm⁻¹, which may suggest the formation of COO-Fe bounds (Caetano-Silva et al., 2017). The Amide II band also reduced in intensity. This intensity reduction may be attributed to the interaction of the amide II groups with the metal ions, as previously reported (Alhazmi, 2019).

A broad band at 3280 cm⁻¹ was observed at the original substrate, which can be attributed to Amine A (Wu et al., 2017). However, in the complex FTIR spectrum, this band has shifted to 3223 cm⁻¹ as a result of the complexation reaction, which strongly supports the claim that peptides have successfully complexed with Fe.

Comparison with the FTIR spectra of Fe precipitates (without peptide supernatant), most likely Fe hydroxides, showed little similarity in the position of the main bands between Fe precipitates and Fe complexes spectra. A broad band can be observed at 3134 cm⁻¹, most likely related to the O-H of the hydroxides in the precipitate, dissimilar to the 3223 cm⁻¹ band on the complex. The presence of sharp peaks at 1110, 1020, 745, 622 and 555 cm-1 in the Fe(OH)ₓ spectrum, which are not present in the complexes spectrum, further confirms the difference between the two.

3.4.4. SEM

The morphological properties of Gpep > 1 and its Fe complexes were analysed using SEM and the results are presented in Fig. 7. Both samples are mostly characterized by rough shape particles with different sizes, which is a common feature when freeze-drying is used as a drying method (Liapis and Bruttini, 2020). However, notable differences were observed in the shape and structure of the particles. Gpep > 1 sample was composed of irregular flat plate-shaped flakes, which is characteristic of amorphous material. In contrast, Gpep > 1-Fe complexes showed some small spherical particles with uneven surface in a compact and fragmented foundation. This observation is consistent with previous studies, which have shown that Fe binding can
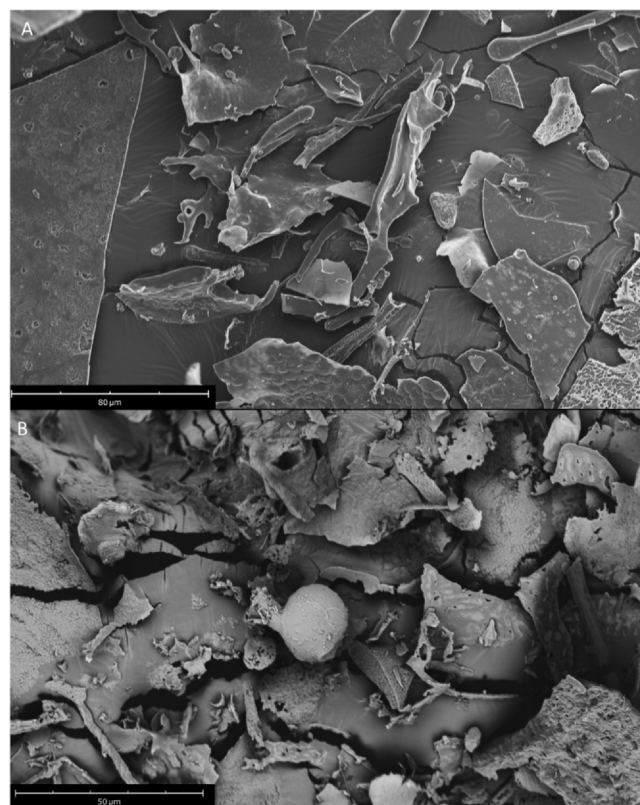
Fig. 7 – Microscopic morphology of Gpep > 1 freeze-dried samples (A) versus freeze-dried Fe-peptide complexes formed with Gpep > 1 (B), using scanning electron microscopy (SEM).

Table 3 – Average ± standard deviation (n = 3) particle size distribution parameters of peptide fraction and peptide complex.

		Gpep > 1 kDa	Gpep -Fe complexes
Particle size parameters (μm)	Dv10	9.12 ± 0.04	0.749 ± 0.001
	Dv50	39.2 ± 0.1	11.1 ± 0.1
	Dv90	83.2 ± 0.3	39.2 ± 0.1

change the original flat peptide plates and result in the formation of spherical structures (Ferreira et al., 2022; Lin et al., 2021; Wang et al., 2020).

3.4.5. Particle size

The particle size distribution of Gpep > 1 kDa and Gpep-Fe complexes were analyzed and the results are shown in Table 3. As particle size is a critical parameter that can affect the flow properties of powders, it is important to understand how the complexation with Fe ions affects the size of the particles. As shown in the table, the median particle size (Dv50) of Gpep > 1-Fe complex were < 11.1 μm, while Gpep > 1 kDa presented particles < 39.1 μm. Similarly, at 90% distribution (Dv90) the Gpep-Fe complexes had particle sizes of 39.2 μm, while Gpep > 1 kDa was found to have particle sizes of < 83.2 μm. These results suggest that the complexation of Gpep > 1 kDa with Fe^{2+} ions leads to a reduction in the particle size, which can be attributed to structural folding and molecular structure rearrangement, which some authors called the "bridging role" between Fe^{2+} and peptides' carboxyl group (Li et al., 2019). The reduction of particle size after complexation can also be confirmed by morphological analysis of Gpep > 1 and Gpep > 1-Fe complexes (Fig. 7), is already been described by other authors (Ferreira et al., 2022; Wang et al., 2020).

4. Conclusion

In summary, this study has demonstrated the potential of waste streams from β-glucan and mannan production processes as a source for eco-friendly Fe-peptide complexes. Through a multifactor factorial experimental design, the optimal conditions for producing these complexes were determined. From a pure mathematical standpoint, the best conditions were pH 6.0 and 1 h of reaction. However, when evaluating reagent consumption and the final yields, a time of 0.5 h was deemed more reasonable. The presence and quality of the complexes was also evaluated by structural and chemical characterization methods. Thus, a new eco-friendly, waste reducing alternative Fe-complex has been formulated and characterized. These findings suggest that these complexes are promising options for Fe supplementation and merit further studies regarding biocompatibility and bioavailability needed to be conducted in order to assess the feasibility of the use of such complexes as Fe supplementation. Additionally, this research also presents a valuable approach to valorizing industrial waste streams and reduces the environmental impact by repurposing them in a sustainable way.

Funding

Declaration of Competing Interest

The authors declare that they have no known competing financial interests or personal relationships that could have appeared to influence the work reported in this paper.

Acknowledgements

Appendix A. Supporting information

Supplementary data associated with this article can be found in the online version at doi:10.1016/j.fbp.2023.06.006.

References

Ahile, U.J., Wuana, R.A., Itodo, A.U., Sha'Ato, R., Dantas, R.F., 2020. Stability of iron chelates during photo-Fenton process: The role of pH, hydroxyl radical attack and temperature. J. Water Process Eng. 36, 101320. https://doi.org/10.1016/j.jwpe.2020.101320

Alhazmi, H., 2019. FT-IR Spectroscopy for the Identification of Binding Sites and Measurements of the Binding Interactions of Important Metal Ions with Bovine Serum Albumin. Sci. Pharm. 87, 5. https://doi.org/10.3390/scipharm87010005

Anderson, G.J., Lu, Y., Frazer, D.M., Collins, J.F., 2018. Intestinal iron absorption. Reference Module in Biomedical Sciences. Elsevier, pp. 1–11. https://doi.org/10.1016/B978-0-12-801238-3.65641-6

AOAC, 2005. Official Methods of Analysis of AOAC International. Association of Official Analysis Chemists International.

Athira, S., Mann, B., Sharma, R., Pothuraju, R., Bajaj, R.K., 2021. Preparation and characterization of iron-chelating peptides from whey protein: an alternative approach for chemical iron fortification. Food Res. Int. 141, 110133. https://doi.org/10.1016/j.foodres.2021.110133

Bombe, K., 2019. Specialty Yeast Market by Type (Yeast Extract, Yeast Autolysate, Yeast Beta - Glucan), Application (Bakery Production, Flavoring, Biofuels), Species (*Saccharomyces Cerevisiae, Kluyveromyces*), and Industry – Global Forecast to 2025 [WWW Document]. URL ⟨https://www.meticulousresearch.com/product/specialty-yeast-market-5032/?utm_source=Globnewswire.com&utm_medium=PressRelease&utm_campaign=Paid⟩.

Budseekoad, S., Yupanqui, C.T., Sirinupong, N., Alashi, A.M., Aluko, R.E., Youravong, W., 2018. Structural and functional characterization of calcium and iron-binding peptides from mung bean protein hydrolysate. J. Funct. Foods 49, 333–341. https://doi.org/10.1016/j.jff.2018.07.041

Caetano-Silva, M.E., Alves, R.C., Lucena, G.N., Frem, R.C.G., Bertoldo-Pacheco, M.T., Lima-Pallone, J.A., Netto, F.M., 2017. Synthesis of whey peptide-iron complexes: influence of using different iron precursor compounds. Food Res. Int. 101, 73–81. https://doi.org/10.1016/j.foodres.2017.08.056

Caetano-Silva, M.E., Bertoldo-Pacheco, M.T., Paes-Leme, A.F., Netto, F.M., 2015. Iron-binding peptides from whey protein hydrolysates: evaluation, isolation and sequencing by LC-MS/MS. Food Res. Int. 71, 132–139. https://doi.org/10.1016/j.foodres.2015.01.008

Caetano-Silva, M.E., Cilla, A., Bertoldo-Pacheco, M.T., Netto, F.M., Alegría, A., 2018. Evaluation of in vitro iron bioavailability in

free form and as whey peptide-iron complexes. J. Food Compos. Anal. 68, 95–100. https://doi.org/10.1016/j.jfca.2017.03.010

Caetano-Silva, M.E., Netto, F.M., Bertoldo-Pacheco, M.T., Alegría, A., Cilla, A., 2020. Peptide-metal complexes: obtention and role in increasing bioavailability and decreasing the pro-oxidant effect of minerals. Crit. Rev. Food Sci. Nutr. 0, 1–20. https://doi.org/10.1080/10408398.2020.1761770

Chatelain, P.G., Pintado, M.E., Vasconcelos, M.W., 2014. Evaluation of chitooligosaccharide application on mineral accumulation and plant growth in Phaseolus vulgaris. Plant Sci. 215–216, 134–140. https://doi.org/10.1016/j.plantsci.2013.11.009

Chen, Q., Guo, L., Du, F., Chen, T., Hou, H., Li, B., 2017. The chelating peptide (GPAGPHGPPG) derived from Alaska pollock skin enhances calcium, zinc and iron transport in Caco-2 cells. Int. J. Food Sci. Technol. 52, 1283–1290. https://doi.org/10.1111/ijfs.13396

Coates, J., 2006. Interpretation of Infrared Spectra, A Practical Approach. Encyclopedia of Analytical Chemistry. John Wiley & Sons, Ltd, Chichester, UK, pp. 1–23. https://doi.org/10.1002/9780470027318.a5606

Collins, J.F., Anderson, G.J., 2012. Molecular mechanisms of intestinal iron transport. Physiology of the Gastrointestinal Tract. Elsevier, pp. 1921–1947. https://doi.org/10.1016/B978-0-12-382026-6.00071-3

Conway, J., 2021. Beer production worldwide from 1998 to 2020 [WWW Document]. URL ⟨https://www.statista.com/statistics/270275/worldwide-beer-production/⟩ (accessed 11.26.21).

de la Hoz, L., Nunes da Silva, V.S., Morgano, M.A., Pacheco, M.T.B., 2014a. Small peptides from enzymatic whey hydrolyzates increase dialyzable iron. Int. Dairy J. 38, 145–147. https://doi.org/10.1016/j.idairyj.2013.12.009

de la Hoz, L., Ponezi, A.N., Milani, R.F., Nunes da Silva, V.S., Sonia de Souza, A., Bertoldo-Pacheco, M.T., 2014b. Iron-binding properties of sugar cane yeast peptides. Food Chem. 142, 166–169. https://doi.org/10.1016/j.foodchem.2013.06.133

Eckert, E., Lu, L., Unsworth, L.D., Chen, L., Xie, J., Xu, R., 2016. Biophysical and in vitro absorption studies of iron chelating peptide from barley proteins. J. Funct. Foods 25, 291–301. https://doi.org/10.1016/j.jff.2016.06.011

Fairweather-Tait, S.J., Teucher, B., 2002. Iron and calcium bioavailability of fortified foods and dietary supplements. Nutr. Rev. 60, 360–367. https://doi.org/10.1301/00296640260385801

Faustino, M., Durão, J., Pereira, C.F., Pintado, M.E., Carvalho, A.P., 2021. Mannans and mannan oligosaccharides (MOS) from Saccharomyces cerevisiae – A sustainable source of functional ingredients. Carbohydr. Polym. 272. https://doi.org/10.1016/j.carbpol.2021.118467

Ferreira, C., Pereira, C.F., Oliveira, A.S., Faustino, M., Pereira, A.M., Durão, J., Pereira, J.O., Pintado, M.E., Carvalho, A.P., 2022. A step for the valorization of spent yeast through production of iron–peptide complexes—a process optimization study. Processes 10, 1464. https://doi.org/10.3390/pr10081464

Freimund, S., Sauter, M., Käppeli, O., Dutler, H., 2003. A new non-degrading isolation process for 1,3-β-D-glucan of high purity from baker's yeast Saccharomyces cerevisiae. Carbohydr. Polym. 54, 159–171. https://doi.org/10.1016/S0144-8617(03)00162-0

Guo, L., Harnedy, P.A., O'Keeffe, M.B., Zhang, L., Li, B., Hou, H., FitzGerald, R.J., 2015. Fractionation and identification of Alaska pollock skin collagen-derived mineral chelating peptides. Food Chem. 173, 536–542. https://doi.org/10.1016/j.foodchem.2014.10.055

Guo, L., Hou, H., Li, B., Zhang, Z., Wang, S., Zhao, X., 2013. Preparation, isolation and identification of iron-chelating peptides derived from Alaska pollock skin. Process Biochem 48, 988–993. https://doi.org/10.1016/j.procbio.2013.04.013

Huang, G., Ren, Z., Jiang, J., 2011. Separation of iron-binding peptides from shrimp processing by-products hydrolysates. Food Bioprocess Technol. 4, 1527–1532. https://doi.org/10.1007/s11947-010-0416-3

Jeppsen, R., Borzelleca, J., 1999. Safety evaluation of ferrous bisglycinate chelate. Food Chem. Toxicol. 37, 723–731. https://doi.org/10.1016/S0278-6915(99)00052-6

Jin, Y.G., Fu, W.W., Ma, M.H., 2011. Preparation and structure characterization of soluble bone collagen peptide chelating calcium. Afr. J. Biotechnol. 10, 10204–10211. https://doi.org/10.5897/ajb10.1923

Lazarte, C.E., Carlsson, N.G., Almgren, A., Sandberg, A.S., Granfeldt, Y., 2015. Phytate, zinc, iron and calcium content of common Bolivian food, and implications for mineral bioavailability. J. Food Compos. Anal. 39, 111–119. https://doi.org/10.1016/j.jfca.2014.11.015

Lee, S.-H., Song, K.Bin, 2009. Purification of an iron-binding nonapeptide from hydrolysates of porcine blood plasma protein. Process Biochem. 44, 378–381. https://doi.org/10.1016/j.procbio.2008.12.001

Li, B., He, H., Shi, W., Hou, T., 2019. Effect of duck egg white peptide-ferrous chelate on iron bioavailability in vivo and structure characterization. J. Sci. Food Agric. 99, 1834–1841. https://doi.org/10.1002/jsfa.9377

Liapis, A., Bruttini, R., 2020. Freeze Drying. In: Handbook of Industrial Drying, pp. 309–343.

Lin, S., Hu, X., Li, L., Yang, X., Chen, S., Wu, Y., Yang, S., 2021. Preparation, purification and identification of iron-chelating peptides derived from tilapia (Oreochromis niloticus) skin collagen and characterization of the peptide-iron complexes. LWT 149, 111796. https://doi.org/10.1016/j.lwt.2021.111796

Liu, X.Y., Wang, Q., Cui, S.W., Liu, H.Z., 2008. A new isolation method of β-d-glucans from spent yeast Saccharomyces cerevisiae. Food Hydrocoll. 22, 239–247. https://doi.org/10.1016/j.foodhyd.2006.11.008

Malison, A., Arpanutud, P., Keeratipibul, S., 2021. Chicken foot broth byproduct: a new source for highly effective peptide-calcium chelate. Food Chem. 345, 128713. https://doi.org/10.1016/j.foodchem.2020.128713

Marson, G.V., de Castro, R.J.S., Belleville, M.P., Hubinger, M.D., 2020. Spent brewer's yeast as a source of high added value molecules: a systematic review on its characteristics, processing and potential applications. World J. Microbiol. Biotechnol. 36, 1–22. https://doi.org/10.1007/s11274-020-02866-7

Monhemius, A.J., 1977. Precipitation diagrams for metal hydroxides, sulphides, arsenates and phosphates. Trans. Inst. Min. Metall. Sect. C. Miner. Process. Extr. Metall. 86.

O'Loughlin, I.B., Kelly, P.M., Murray, B.A., FitzGerald, R.J., Brodkorb, A., 2015. Molecular characterization of whey protein hydrolysate fractions with ferrous chelating and enhanced iron solubility capabilities. J. Agric. Food Chem. 63, 2708–2714. https://doi.org/10.1021/jf505817a

Oliveira, A.S., Ferreira, C., Pereira, J.O., Pintado, M.E., Carvalho, A.P., 2022a. Spent brewer's yeast (Saccharomyces cerevisiae) as a potential source of bioactive peptides: An overview. Int. J. Biol. Macromol. 208, 1116–1126. https://doi.org/10.1016/j.ijbiomac.2022.03.094

Oliveira, A.S., Ferreira, C., Pereira, J.O., Pintado, M.E., Carvalho, A.P., 2022b. Valorisation of protein-rich extracts from spent brewer's yeast (Saccharomyces cerevisiae): an overview. Biomass-.-. Convers. Biorefinery. https://doi.org/10.1007/s13399-022-02636-5

Oliveira, A.S., Pereira, J.O., Ferreira, C., Faustino, M., Durão, J., Pintado, M.E., Carvalho, A.P., 2022c. Peptide-rich extracts from spent yeast waste streams as a source of bioactive compounds for the nutraceutical market. Innov. Food Sci. Emerg. Technol. 81, 103148. https://doi.org/10.1016/j.ifset.2022.103148

Onufriev, A.V., Alexov, E., 2013. Protonation and pK changes in protein–ligand binding. Q. Rev. Biophys. 46, 181–209. https://doi.org/10.1017/S0033583513000024

Safiri, S., Kolahi, A.A., Noori, M., Nejadghaderi, S.A., Karamzad, N., Bragazzi, N.L., Sullman, M.J.M., Abdollahi, M., Collins, G.S., Kaufman, J.S., Grieger, J.A., 2021. Burden of anemia and its underlying causes in 204 countries and territories, 1990–2019: results from the Global Burden of Disease Study 2019. J. Hematol. Oncol. 14, 185. https://doi.org/10.1186/s13045-021-01202-2

Shubham, K., Anukiruthika, T., Dutta, S., Kashyap, A.V., Moses, J.A., Anandharamakrishnan, C., 2020. Iron deficiency anemia: a comprehensive review on iron absorption, bioavailability

and emerging food fortification approaches. Trends Food Sci. Technol. 99, 58–75. https://doi.org/10.1016/j.tifs.2020.02.021

Smialowska, A., Matia-Merino, L., Carr, A.J., 2017. Assessing the iron chelation capacity of goat casein digest isolates. J. Dairy Sci. 100, 2553–2563. https://doi.org/10.3168/jds.2016-12090

Sun, N., Cui, P., Jin, Z., Wu, H., Wang, Y., Lin, S., 2017. Contributions of molecular size, charge distribution, and specific amino acids to the iron-binding capacity of sea cucumber (Stichopus japonicus) ovum hydrolysates. Food Chem. 230, 627–636. https://doi.org/10.1016/j.foodchem.2017.03.077

Tian, X., Yang, P., Jiang, W., 2019. Effect of alkali treatment combined with high pressure on extraction efficiency of β-d-Glucan from spent Brewer's yeast. Waste Biomass Valoriz. 10, 1131–1140. https://doi.org/10.1007/s12649-017-0130-8

Torres-Fuentes, C., Alaiz, M., Vioque, J., 2012. Iron-chelating activity of chickpea protein hydrolysate peptides. Food Chem. 134, 1585–1588. https://doi.org/10.1016/j.foodchem.2012.03.112

Waldvogel-Abramowski, S., Waeber, G., Gassner, C., Buser, A., Frey, B.M., Favrat, B., Tissot, J.-D., 2014. Physiology of iron metabolism. Transfus. Med. Hemotherapy 41, 213–221. https://doi.org/10.1159/000362888

Walters, M., Esfandi, R., Tsopmo, A., 2018. Potential of food hydrolyzed proteins and peptides to chelate iron or calcium and enhance their absorption. Foods 7, 172. https://doi.org/10.3390/foods7100172

Wang, L., Ding, Y., Zhang, X., Li, Yongfu, Wang, R., Luo, X., Li, Yanan, Li, J., Chen, Z., 2018. Isolation of a novel calcium-binding peptide from wheat germ protein hydrolysates and the prediction for its mechanism of combination. Food Chem. 239, 416–426. https://doi.org/10.1016/j.foodchem.2017.06.090

Wang, T., Lin, S., Cui, P., Bao, Z., Liu, K., Jiang, P., Zhu, B., Sun, N., 2020. Antarctic krill derived peptide as a nanocarrier of iron through the gastrointestinal tract. Food Biosci. 36, 100657. https://doi.org/10.1016/j.fbio.2020.100657

WHO, 2021. Anaemia in women and children [WWW Document]. https//www.who.int/data/gho/data/themes/topics/anaemia_in_women_and_children, Assess. 10th June 2021. URL ⟨https://www.who.int/data/gho/data/themes/topics/anaemia_in_women_and_children⟩ (accessed 3.29.22).

World Health Organization, 2008. Worldwide prevalence of anaemia 1993–2005.

Wu, H., Liu, Z., Zhao, Y., Zeng, M., 2012. Enzymatic preparation and characterization of iron-chelating peptides from anchovy (Engraulis japonicus) muscle protein. Food Res. Int. 48, 435–441. https://doi.org/10.1016/j.foodres.2012.04.013

Wu, W., Li, B., Hou, H., Zhang, H., Zhao, X., 2017. Identification of iron-chelating peptides from Pacific cod skin gelatin and the possible binding mode. J. Funct. Foods 35, 418–427. https://doi.org/10.1016/j.jff.2017.06.013

Wu, W., Yang, Y., Sun, N., Bao, Z., Lin, S., 2020. Food protein-derived iron-chelating peptides: the binding mode and promotive effects of iron bioavailability. Food Res. Int. 131, 108976. https://doi.org/10.1016/j.foodres.2020.108976

Yang, Y.Z., Li, M.J., Zhou, B.B., Zhang, Q., Li, X.L., Zhang, J.K., Wei, Q.P., 2019. Synthesis, characterization, and evaluation of bioactivity of novel Fe(II) nano-complexes based on sucrose, glucose, and fructose. Chem. Pap. 73, 321–329. https://doi.org/10.1007/s11696-018-0582-8

Yuan, B., Zhao, C., Cheng, C., Huang, D., Cheng, S., Cao, C., Chen, G., 2019. A peptide-Fe(II) complex from Grifola frondosa protein hydrolysates and its immunomodulatory activity. Food Biosci. 32, 100459. https://doi.org/10.1016/j.fbio.2019.100459

Zhang, L.Y., Li, X.F., Liao, X.D., Zhang, L.Y., Lu, L., Luo, X.G., 2017. Effect of iron source on iron absorption and gene expression of iron transporters in the ligated duodenal loops of broilers. J. Anim. Sci. 95, 1587. https://doi.org/10.2527/jas2016.1147

Zhang, Y., Ding, X., Li, M., 2021. Preparation, characterization and in vitro stability of iron-chelating peptides from mung beans. Food Chem. 349, 129101. https://doi.org/10.1016/j.foodchem.2021.129101

Zhou, J., Wang, X., Ai, T., Cheng, X., Guo, H.Y., Teng, G.X., Mao, X.Y., 2012. Preparation and characterization of β-lactoglobulin hydrolysate-iron complexes. J. Dairy Sci. 95, 4230–4236. https://doi.org/10.3168/jds.2011-5282

Zhu, X., Zou, R., Sun, P., Wang, Q., Wu, J., 2018. A supramolecular peptide polymer from hydrogen-bond and coordination-driven self-assembly. Polym. Chem. 9, 69–76. https://doi.org/10.1039/C7PY01901G